Structure and Organization of Bacteriophage Pf3 Probed by Raman and Ultraviolet Resonance Raman Spectroscopy†

Zai Qing Wen,‡ Stacy A. Overman, Priya Bondre, and George J. Thomas, Jr.*

Division of Cell Biology and Biophysics, School of Biological Sciences, University of Missouri−Kansas City, Kansas City, Missouri 64110

Received August 10, 2000; Revised Manuscript Received November 6, 2000

ABSTRACT: The *Pseudomonas* bacteriophage Pf3 is a long and narrow filament consisting of a covalently closed DNA single strand of 5833 bases sheathed by ∼2500 copies of a 44-residue subunit. Ultraviolet resonance Raman spectra excited at 257, 244, 238, and 229 nm and off-resonance Raman spectra excited at 514.5 nm are reported for Pf3 in both H_2O and D_2O solutions. The key Raman bands are assigned to specific protein and DNA groups of the native virion assembly. The results are compared with proposed assembly models and Raman spectra recently reported for the isomorphous (class II) *Pseudomonas* phage Pf1 and the morphologically distinct (class I) coliphage fd [Wen, Z. Q., Overman, S. A., and Thomas, G. J., Jr. (1997) *Biochemistry 36,* 7810−7820; Wen, Z. Q., Armstrong, A., and Thomas, G. J., Jr. (1999) *Biochemistry 38,* 3148−3156]. Surprisingly, deoxynucleosides of the packaged DNA genome of Pf3 adopt the same conformation (C3′-*endo*/*anti*) found for DNA packaged in the class I fd virion rather than that (C2′-*endo*/*anti*) associated with DNA in the isomorphous Pf1 virion. However, DNA base stacking in Pf3, as judged by Raman hypochromic effects, differs significantly from that occurring in either Pf1 or fd. Thus, the single-stranded DNA genomes of Pf3, Pf1, and fd are all organized differently within their respective capsids, implying that local subunit−DNA interactions may be important in determining the structure specific to each native assembly. The present study confirms a completely α-helical secondary structure for the Pf3 subunit and an unusual indolyl ring environment for the subunit tryptophan residue (Trp-38).

Pf3 is a filamentous bacteriophage that infects strains of *Pseudomonas aeruginosa* harboring the RP1 plasmid. The Pf3 virion comprises a covalently closed DNA single strand of 5833 nucleotides, encapsidated by ∼2500 copies of a 44-residue major coat protein subunit plus a few copies of minor coat proteins at the filament ends (*1*). The tubular capsid represents about 87% of the virion mass. Fiber X-ray diffraction shows that the major coat protein is arranged in a single-start helix of approximately 5.4 subunits per turn (class II symmetry, $C_1S_{5.4}$), which is similar to the architecture of the *Pseudomonas* phage Pf1 (*1*−*3*). This is distinct from the class I symmetry (C_5S_2) of the coliphages Ff (strains fd, f1, and M13), IKe, and If1 wherein the coat protein is assembled as a five-start helix with 10 subunits per helical turn (*1*, *4*, *5*).

Although the coat subunit of every known filamentous virus is small and highly α-helical, the Pf3 subunit is unusual in several respects (sequence: MQSVITDVTG[10] QLTAVQA-DIT[20] TIGGAIIVLA[30] AVVLGIRWIK[40] AQFF). Importantly, it is synthesized without an N-terminal leader, a characteristic that has favored study of the Pf3 assembly mechanism as a model for membrane protein insertion and translocation (*6*, *7*). Tandem C-terminal phenylalanines (Phe-43, Phe-44) and the absence of tyrosine are also unique to the Pf3 subunit sequence. An essential tryptophan (Trp-38) located between two basic residues (Arg-37 and Lys-40) and near the C terminus is a characteristic found only in coat proteins of the class II phages, Pf3 and Xf (*1*).

A recently proposed 3.1-Å model for the arrangement of subunits in the Pf3 capsid (*2*) provides a convenient starting point for evaluating intra- and intersubunit contacts and assessing possible subunit interactions with the packaged single-stranded DNA (ssDNA)[1] genome. However, because of both the low resolution of the fiber electron density map and the absence of diffraction from packaged DNA, key details of side-chain orientations, nucleotide conformations and local residue environments were not resolved. Such structural features can be revealed by Raman and ultraviolet resonance Raman (UVRR) probes (*8*−*11*). Previous Raman and UVRR applications to both class I (fd) and class II (Pf1) viruses (reviewed in ref *8*) demonstrate the complementarity of fiber spectroscopic and diffraction results, which together enable more accurate modeling of protein−protein and protein−DNA interactions in these assemblies (*9*, *10*). Here, we apply Raman and UVRR probes to Pf3.

UVRR spectra have been obtained using four different laser excitation wavelengths—229, 238, 244, and 257 nm—all of which are within the broad UV absorption profile of the Pf3 virion. As shown previously (*11*−*14*), 229 nm excitation results in spectral domination by Raman markers of tryptophan, whereas 257 nm excitation promotes Raman

† Supported by NIH Grant GM50776.

* To whom correspondence should be addressed. Telephone: (816)-235-5247. Fax: (816)235-1503. E-mail: thomasgj@umkc.edu.

‡ Present address: Department of Process Development, Amgen, Inc., Thousand Oaks, CA.

[1] Abbreviations: ssDNA, single-stranded DNA; dsDNA, double-stranded DNA; UVRR, ultraviolet resonance Raman.

10.1021/bi0018887 CCC: $20.00
Published on Web 12/12/2000

markers of the ssDNA bases. Accordingly, these UVRR spectra provide a means for selectively monitoring in Pf3 either the Trp-38 residue of the coat subunit or the deoxynucleoside base residues of the packaged genome. Raman markers of both Trp-38 and DNA bases are resolved in the 238- and 244-nm excited UVRR spectra. The prolific off-resonance Raman spectrum (514.5 nm excitation) consists of approximately 60 discrete Raman bands, representing vibrational signatures of both coat subunit and packaged ssDNA molecules.

The specific objectives of this work are the following: (i) Establish comprehensive Raman and UVRR vibrational band assignments for Pf3, consistent with previously proposed assignments for fd (*12*, *13*) and Pf1 (*14*). Such assignments are essential for the structural interpretations presented here and in related UVRR (*11*) and polarized Raman (*15*) analyses of Pf3. (ii) Develop structural interpretations for the Raman and UVRR markers of Pf3 coat protein and DNA to complement and extend those proposed in previous fiber diffraction and model building studies (*1*, *2*). (iii) Identify structural features of Pf3 that may distinguish it from class I and other class II phages.

MATERIALS AND METHODS

Sample Preparations. Pf3 was grown on *P. aeruginosa* (strain PAO1 bearing the RP1 plasmid) in LB medium using stocks obtained originally from Dr. Loren A. Day, Public Health Research Institute, New York, NY. Growth media constituents were purchased from Sigma (St. Louis, MO). D_2O (99.9%) was obtained from Aldrich (Milwaukee, WI). Mature viral particles, extruded through the bacterial membrane and into the growth medium, were collected by poly(ethylene glycol) precipitation followed by low speed centrifugation. The virus particles were purified by repeated cycles of centrifugation (330000*g*) in 10 mM Tris (pH 7.8) to yield a pellet from which virus solutions were prepared for Raman analyses. Further details of the isolation and purification procedures for spectroscopic analysis of filamentous viruses have been described (*11*−*14*, *16*).

Aqueous solutions were prepared for off-resonance Raman spectroscopy by resuspension of the virus in 10 mM Tris (pH 7.8) at concentrations in the range of 10−100 mg/mL. Solutions for UVRR and fluorescence spectroscopy were prepared by resuspension of the virus in the same buffer at 0.4 mg/mL and 2.7 μg/mL, respectively. Deuterated Pf3 was prepared identically, except that D_2O (pD 7.8) replaced H_2O in the pelleting and dilution buffers. Pf3 concentrations were determined by UV absorption assuming a virion extinction coefficient of 4.53 cm^2/mg at 264 nm (*1*). Sodium sulfate (Na_2SO_4) was added at precisely determined concentrations to sample solutions for use of its Raman band at 981 cm^{-1} as an internal intensity standard.

Raman Spectroscopy. For off-resonance Raman spectroscopy, the sample solution was sealed in a glass capillary (KIMAX 34507). Spectra were excited at 514.5 nm and collected on a single grating spectrometer (Spex 500M, Instruments S.A., Edison, NJ) equipped with a liquid nitrogen-cooled charge-coupled device detector. The effective spectral resolution is 3.5 cm^{-1}. Raman frequencies were calibrated to $\pm$1 cm^{-1} with indene and CCl_4 liquids. Laser power at the sample was maintained at or below 200 mW. The total acquisition time for each spectrum was about 30 min. Other details of Raman data collection have been described (*17*).

UVRR Spectroscopy. For UVRR spectroscopy, the sample solution was sealed in a custom-designed cylindrical quartz cell and rotated at 3000 rpm. Spectra were excited at 229, 238, 244, and 257 nm with a continuous-wave, frequency-doubled argon laser (Innova 300 FReD, Coherent Inc., Santa Clara, CA) using a radiant power at the sample cell of 1 mW or less for 229, 238, and 244 nm excitations and 5 mW or less for 257 nm excitation. Raman scattering at 90° was analyzed using a single-grating (2400 g/mm) spectrograph (Spex 750M, Instruments, S.A.) equipped with a prism predispersive element (McPherson Instruments, Acton, MA) and liquid nitrogen-cooled, charge-coupled device detector (Instruments, S.A.). The effective spectral resolution is 8 cm^{-1} or less. Further details of the design and performance of the UVRR spectrometer have been described (*18*).

UVRR frequencies were calibrated to $\pm$1 cm^{-1} using acetonitrile liquid and/or an internal standard (Na_2SO_4). The spectra shown below represent an average of six data collections, each acquired during an exposure of 1 h or less. Interfering cosmic rays and weak Raman scattering of the aqueous buffer and quartz cell were removed as previously described (*18*, *19*). Spectral differences were computed to verify that each sample showed no significant time dependence of its UVRR spectrum. Consistent with demonstrated characteristics of the UVRR spectrometer, no sample photodecomposition occurred during the data collection protocols. Sample integrity was also confirmed by UV absorption spectroscopy following UVRR data collections.

Fluorescence Spectroscopy. Fluorescence emission spectra were collected on a Bowman series 2 fluorescence spectrometer (SLM Instruments, Urbana, IL) using 295 nm excitation. The bandwidth of excitation and emission slits was 2 nm.

Data Analysis. (*a*) *Raman Scattering Cross Sections*. The scattering cross section (σ_n) of a Raman band of frequency ν_n is obtained by comparison of its peak height (I_n) with the peak height (I_s) of an internal standard Raman band (ν_s) of known scattering cross section (σ_s) by use of

$$\sigma_n = \sigma_s(I_n/I_s)(C_s/C_n)[(\nu_0 - \nu_s)/(\nu_0 - \nu_n)]^4 \qquad (1)$$

where C_s and C_n are the molar concentrations of the internal standard and target species, respectively, and ν_0 is the frequency of the exciting line, expressed in cm^{-1}. Here, we employ as internal standard the prominent UVRR band of sodium sulfate at 981 cm^{-1}. Fodor et al. (*20*) have determined the absolute Raman scattering cross section of the 981 cm^{-1} band of SO_4^{2-} as a function of excitation wavelength in the ultraviolet region. Using those results, we have σ_s = 0.42, 0.32, 0.24, and 0.16 mb at 229, 238, 244, and 257 nm, respectively. In applying eq 1 to a Raman band of a particular nucleoside constituent of DNA, we replace C_n by C_b ($\equiv X_bC_n$, where X_b is the base mole fraction). C_b is estimated from the UV absorbance of the DNA at 260 nm. For the packaged genome of Pf3, the molar concentration of a particular base is obtained from

$$C_b = X_bC_n = X_bWf/M_{nuc} \qquad (2)$$

where W is the weight concentration of the virion, which can be determined from the UV absorption spectrum and

Table 1: Base Compositions and UV Extinction Coefficients of Pf3 Virus, ssDNA, and dsDNA

	Pf3	ssDNA[a]	dsDNA[b]
wt % DNA	14	100	100
base composition			
%A	20	25	28
%T	35	34	28
%G	24	21	22
%C	21	20	22
av nucleotide mol wt	323	323	323
extinction at λ_{max}	4.53[c]	7200[d]	6300[d]
λ_{max} (nm)	264	260	260

[a] Extracted from fd virus. [b] Extracted from calf thymus nucleohistones. [c] Units of cm^2/mg (see ref *1*). [d] Units of M (phosphate)$^{-1}$ cm^{-1} (from refs *12*, *14*, and *19* and references therein).

known extinction coefficients; f is the nominal weight fraction of DNA in the virion; and M_{nuc} is the average nucleotide molecular weight. The appropriate information to apply eqs 1 and 2 to the DNA-containing samples investigated here is given in Table 1. In evaluating the Raman cross section of a tryptophan band of Pf3, we make use of the known subunit/nucleotide ratio (1:2.4) and the presence of one tryptophan per subunit (*1*) to obtain C_w:C_n = 1:2.4. As in previous applications of the UVRR method to filamentous viruses (*12*, *14*), the present data are uncorrected for the presumably negligible effects of protein and DNA chromophores on their respective Raman cross sections. Such effects are assumed to be completely and correctly compensated by normalization to the UVRR scattering cross section of the Na_2SO_4 standard present in all solutions.

(*b*) *Raman Hypochromic Effects*. We define the fractional hypochromicity of a DNA Raman band at frequency ν_n as 1 − γ_n, where the hypochromic ratio, γ_n, is the quotient of intensities in Raman spectra of the nucleic acid and constituent nucleosides. In terms of the corresponding Raman scattering cross sections:

$$\gamma_n^{DNA} \equiv I_n^{DNA}/I_n^{nuc} = \sigma_n^{DNA}/\sigma_n^{nuc} \quad (3)$$

where σ_n^{DNA} and σ_n^{nuc} are Raman scattering cross sections for the band in DNA and in a solution of the free nucleoside, respectively. By analogy with eq 3, we define γ_n^{prot} for a Raman band of a protein aromatic residue as

$$\gamma_n^{prot} \equiv I_n^{prot}/I_n^{aa} = \sigma_n^{prot}/\sigma_n^{aa} \quad (4)$$

where σ_n^{prot} and σ_n^{aa} are Raman scattering cross sections for the residue in the protein and in a solution of the free amino acid.

(*c*) *Experimental Uncertainties*. The Raman scattering cross sections reported below are averages of multiple independent experiments exhibiting deviations of less than ±10%. These limits of error reflect deviations in band intensity measurements, which are due mainly to spectral noise and baseline uncertainties. Other potential sources of error, such as spectrograph polarization effects and sample photodecomposition, are virtually eliminated by the experimental design and data collection protocols, as previously described (*11*−*14*, *18*, *19*).

RESULTS

Figure 1 indicates the laser wavelengths employed for excitation of UVRR and off-resonance Raman spectra in relation to the UV and visible absorption profile of Pf3. Figure 2 shows the off-resonance (514.5 nm excitation) Raman spectra of Pf3 in H_2O and D_2O solutions, as well as the spectral difference computed by subtraction of the H_2O solution spectrum (subtrahend) from the D_2O solution spectrum (minuend). UVRR spectra (229, 238, 244, and 257 nm excitations) of H_2O and D_2O solutions are shown in Figure 3. The Raman band assignments generated from these data are listed in Table 2.

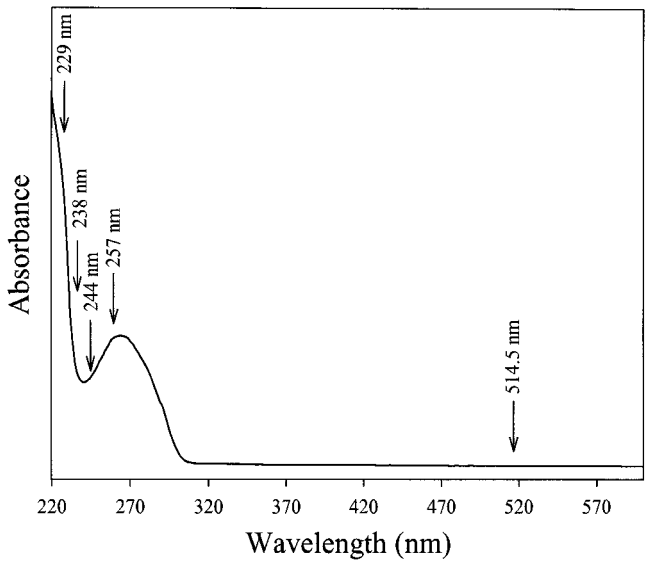

FIGURE 1: Absorption spectrum of Pf3 virus in the wavelength interval 220−600 nm. Arrows indicate the laser wavelengths used to excite the UVRR and off-resonance Raman spectra displayed in subsequent figures. Pf3 concentration is approximately 0.2 mg/mL in 10 mM Tris (pH 7.5), and the optical path is 10 mm.

Key Raman markers of deoxynucleoside conformations in the packaged Pf3 genome are shown in Figure 4. Figure 5 compares the 257-nm UVRR signature of Pf3 with that of a mixture of deoxynucleosides having the same base composition. These UVRR data provide the basis for calculating DNA hypochromicities, which are summarized in Table 3.

DISCUSSION

The off-resonance Raman spectrum of Pf3 is dominated, as expected, by bands of the coat protein. Most of these Raman bands exhibit little or no shift with the change of solvent from H_2O to D_2O, as revealed by the difference spectrum of Figure 2 and corresponding data of Table 2 (columns 1 and 2). Notable exceptions are the conspicuous deuteration effects observed in the intervals 1200−1300 cm^{-1} (amide III region) of the H_2O solution spectrum and 900−980 cm^{-1} (amide III′ region) of the D_2O solution spectrum. These reflect partial exchange of the peptide main chain of the coat subunit. However, the residual amide III intensity at 1270−1275 cm^{-1} in the D_2O solution spectrum as well as the modest amide I (1649 cm^{-1}) → amide I′ (1648 cm^{-1}) shift confirm that peptide exchange is incomplete (∼50%) at the experimental conditions employed. In addition, deuteration-sensitive bands assigned to bases of encapsidated Pf3 DNA, including markers of adenine (726 cm^{-1}) and guanine (1486 and ∼1682 cm^{-1}), exhibit the wavenumber shifts expected for deuteration of base amino and imino groups. Deuteration-sensitive bands of the Trp-38 side chain,

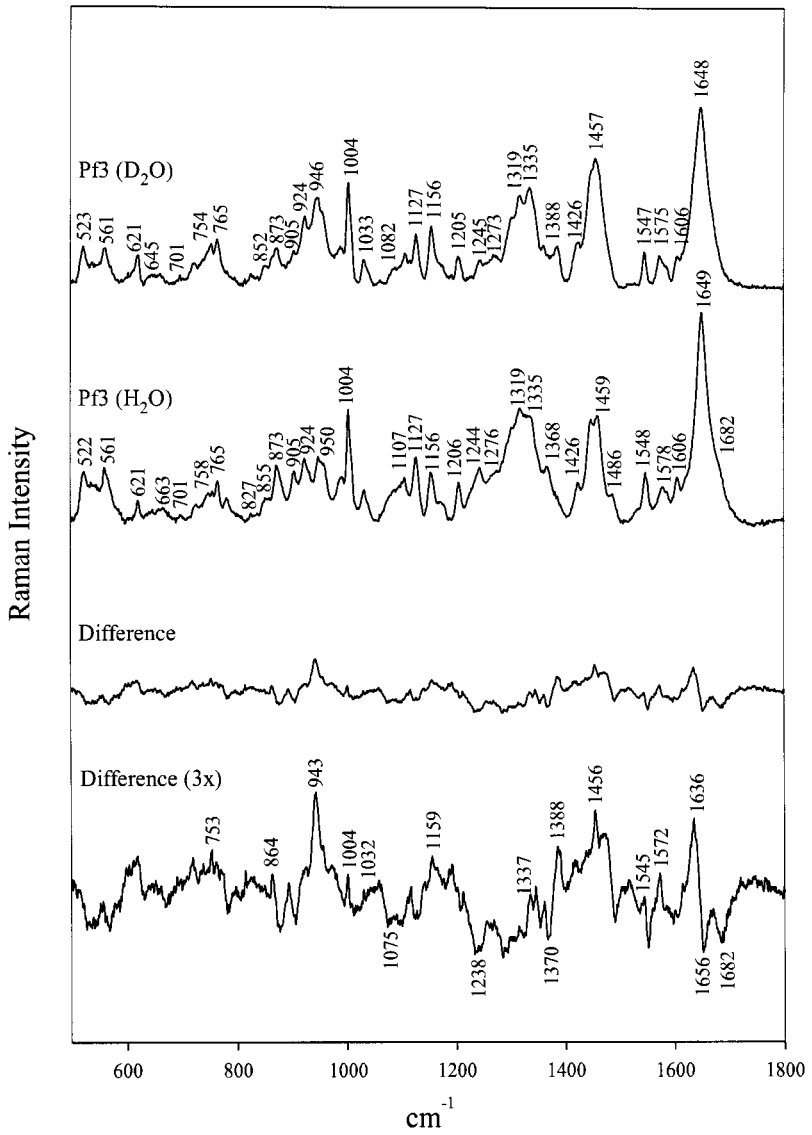

FIGURE 2: Raman spectra (514.5 nm excitation) of Pf3 virus (20 °C) dissolved at 10 mg/mL in 10 mM Tris/H_2O, pH 7.5 (second trace from top) and 10 mM Tris/D_2O, pD 7.5 (top trace) and their difference spectrum (second trace from bottom). A 3-fold amplification of the difference spectrum is also shown (bottom trace). Labels indicate prominent bands discussed in the text. Spectral intensities are normalized to the phenylalanine marker band at 1004 cm^{-1}.

including indolyl ring modes *W18* (763 → 759 cm^{-1}), *W17* (874 → 863 cm^{-1}), *W13* (1130 → 1124 cm^{-1}), *W7* (1368 → 1360 cm^{-1}), *W2* (1581 → 1573 cm^{-1}) and *W1* (1620 → 1614 cm^{-1}), are more clearly apparent in the 229- and 238-nm excited UVRR spectra of Figure 3. Collectively, these results demonstrate that peptide NH → ND exchange is highly protected in the Pf3 capsid; conversely, exchanges of base amino and imino sites in packaged Pf3 DNA and of the indolyl N1H site of Trp-38 in the capsid subunit are relatively unprotected.

UVRR spectra of H_2O and D_2O solutions of Pf3 shown in Figure 3 are in accord with the off-resonance results of Figure 2. As in previous UVRR studies of filamentous viruses (*12*, *14*), the 229-nm excited UVRR spectrum of Pf3 is dominated by bands of tryptophan, whereas the 257-nm spectrum is dominated by bands of the DNA bases. Detailed assignments for the off-resonance and UVRR bands of Pf3 (Table 2) are based upon extensive studies of model compounds (*19*−*21*) and isotopically labeled fd and Pf1 filamentous viruses (*12*−*14*, *16*, *17*, *23*, *24*). The structural significance of several of these assignments is further discussed in the following sections.

Structural Interpretation for Raman Markers of the Pf3 Capsid Subunit. (*a*) *Amide I and Amide III Bands as Indicators of Subunit Secondary Structure*. The strong and sharp amide I band centered at 1649 cm^{-1} (Figure 2, middle trace) indicates a highly α-helical secondary structure for the coat protein subunit. The bandwidth (full width at half-maximum ∼30 cm^{-1}) is comparable to amide I bandwidths observed for fd and Pf1 virions (*12*, *14*, *16*, *25*) and indicates minimal nonhelical secondary structure. [The noticeably greater bandwidth of ∼40 cm^{-1} for amide I′ in the D_2O solution spectrum (Figure 2, top trace) reflects partial deuteration (NH → ND) of amide sites in capsid subunits, as noted above.] The intense amide I band is flanked by weaker bands of lower (1606 and 1621 cm^{-1}) and higher wavenumber (∼1682 cm^{-1}). On the basis of present UVRR data (Figure 3) and observed deuteration effects (Figure 2), these can be assigned respectively to phenylalanine, tryptophan, and glutamine side chains of the coat subunit rather

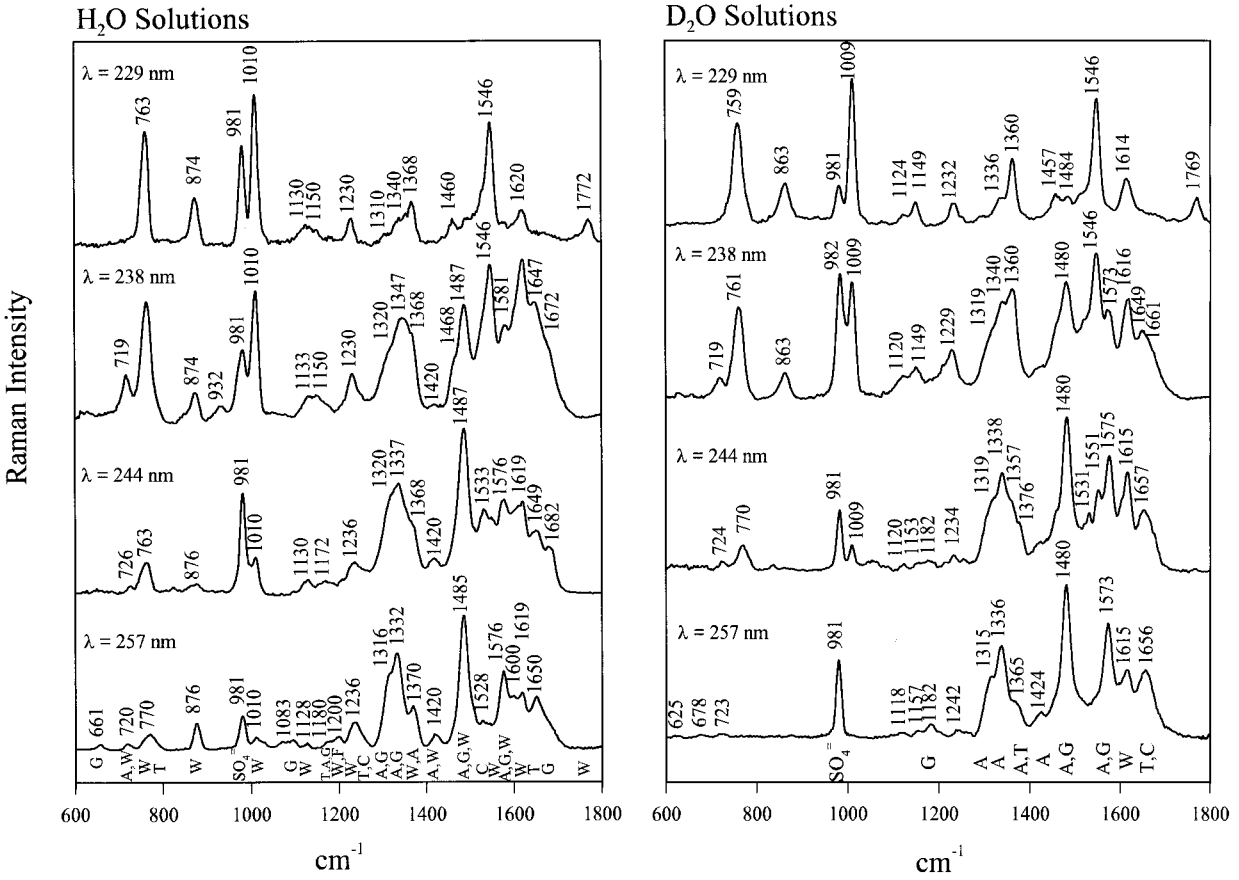

FIGURE 3: Left panel, from top to bottom: UVRR spectra (229, 238, 244, and 257 nm excitations) of Pf3 in H_2O solutions containing 10 mM Tris (pH 7.5) and Na_2SO_4 internal standard. Virus concentrations in terms of moles of DNA nucleotides packaged are 0.17, 0.26, 0.42, and 1.04 mM (1 mM nucleotide = 2.3 mg of Pf3/mL), and corresponding Na_2SO_4 concentrations are 250, 55, 74, and 91 mM, respectively. Right panel, from top to bottom: UVRR spectra (229, 238, 244, and 257 nm excitations) of Pf3 in D_2O solutions containing 10 mM Tris (pD 7.5) and Na_2SO_4 internal standard. Virus concentrations in terms of moles of DNA nucleotides packaged are 0.22, 0.19, 0.87, and 0.56 mM, and corresponding Na_2SO_4 concentrations are 100, 125, 63, and 80 mM, respectively. All data were obtained at 20 °C.

than to any nonhelical components of the peptide backbone. A previous quantitative assessment of subunit α-helicity (>82%), which was based upon Fourier deconvolution of amide I (*25*), thus represents a conservative lower limit. The 1682 cm^{-1} shoulder is not part of an amide I complex but is due primarily to the carbonyl stretching vibrations of residues Gln-2, Gln-11, Gln-16, and Gln-42. (A small contribution near 1680 cm^{-1} is also expected from guanine carbonyl groups of packaged DNA.) Accordingly, the earlier deconvolution result (*25*) reflects ~100% α-helix in the coat subunit. Application of a reference intensity algorithm (*26*) to the amide I band also confirms 90−100% α-helical secondary structure for the coat subunit.

It is also of interest to note that the data of Figures 2 and 3 demonstrate that Pf3 bands near 1235−1245 cm^{-1} are not likely to be part of an amide III complex, but are due to deoxynucleotide bases of packaged ssDNA. Therefore, the amide III profile of the Pf3 capsid consists only of α-helical markers between 1270 and 1310 cm^{-1}, in full accord with the amide I findings: The coat subunit is essentially completely α-helical. The Raman amide I and amide III markers of Figure 2 and the supporting UVRR evidence from Figure 3 constitute a firm experimental foundation for the use of a uniformly α-helical subunit as the basis for model building studies of the Pf3 capsid (*2*).

(*b*) *Raman Bands of Trp-38 and the Environment of the Indolyl Ring*. Wen and Thomas (*11*) recently reported an unusual pattern of UVRR markers specific to the indolyl ring of Trp-38 in the assembled Pf3 virion. The present results confirm the anomalous pattern of Trp-38 Raman markers for both off-resonance and resonance Raman spectra of native Pf3. In particular, the 229-nm excited Raman bands at 763 (*W18*), 874 (*W17*), 1230 (*W10*), 1368 (*W7*), and 1772 cm^{-1} (*W18* + *W16*) are displaced significantly from their counterparts in disassembled Pf3 subunits and in most other tryptophan-containing proteins (*11*). The tryptophan Raman markers of Pf3 differ also from those of the single tryptophan residue (Trp-26) of fd. The anomaly has been attributed to an interaction of the Trp-38 indolyl moiety that is specific to the assembled Pf3 virion. A cation−π interaction (*27*) involving an electropositive group (cation donor) and the indolyl ring (π-electron acceptor) has been proposed (*11*). More recently, a polarized Raman study of the orientation of the Trp-38 indolyl ring in oriented Pf3 (*15*) confirms the steric feasibility of an intrasubunit cation−π interaction between the guanido group of Arg-37 and the Trp-38 indole. Additional structural information may be derived from the Raman markers of Trp-38 that appear prominently in spectra of Figures 2 and 3. Detailed discussions have been given previously (*11*).

(*c*) *Raman Bands of the Guanido Group of Arg-37*. To further test the hypothesis of an Arg-37/Trp-38 cation−π interaction in Pf3 (*11*) and additionally to provide a plausible spectroscopic probe of similar cation−π interactions in other

Table 2: Raman Band Frequencies, Intensities, and Assignments for Filamentous Virus Pf3[a]

excitation wavelength (nm)					
514.5	257	244	238	229	assignment[b]
348 (0)					
377 (0)					
410 (0)					
428 (0B) [426]					
523 (2) [522]					
540 (1B) [540]					
561 (2) [561]					
621 (1) [621]					F (*F6b*)
644 (0) [645]					dT, M
663 (0) [655]	661 [655]				dG
701 (0) [701]					
726 (1) [723]	720 [723]	726 [724]	719 [719]		dA
748 (1) [746]					amIV[IV′], I, L
758 (2) [754]					dT, A, F
765 (3) [765]	770	763 [770]	763 [761]	763 [759]	W (*W18*)
782 (1) [782]					dC, dT
802 (0B) [798]					bk
827 (0) [827]					F (*F1*), OPO s
855 (0) [852]					CCN s,b
873 (2) [873]	874	874	874 [863]	874 [863]	W (*W17*), I, V
905 (2) [905]					A (CC s)
924 (2) [924]					CCN s,b
950 (2) [946]					V, L, amIII′
958 (S) [958]					L
991 (2) [991]					I
1004 (4) [1004]					F (*F12*)
1010 (S) [1010]	1010 [1010]	1010 [1010]	1010 [1010]	1010 [1010]	W (*W16*)
1032 (1) [1033]					F (*F18a*)
1041 (0S) [1042]					T
1082 (S) [1082]	1083				PO_2^-, R (NCN s), dG
1107 (2) [1104]					A, dA
1127 (3) [1127]	1128 [1118]	1130 [1120]	1133 [1120]	1130 [1124]	W (*W13*), I, V, L
1156 (2) [1156]	[1157]	[1153]	1150 [1149]	1150 [1149]	W (*W12?*), I, V
1174 (1) [1174]	1180 [1182]	1172 [1182]			dT, dA, dG
1206 (2) [1205]	1200				W (*W11?*), F (*F7a*)
1230 (S)			1230 [1229]	1230 [1232]	W (*W10*)
1244 (2) [1245]	1236 [1242]	1236 [1234]			dT, dC
1276 (2B) [1273]					amIII, dT, dA
1305 (4S) [1304]					amIII, dA
1319 (4) [1319]	1316 [1315]	1320 [1319]	1320 [1319]	1310	dA, dG, CH b
1335 (3B) [1335]	1332 [1336]	1337 [1338]			$CC^{\alpha}H$ b, dA, dG
			1347 [1340]	1340 [1336]	W (*W7′*)
1368 (2) [1362]	1370 [1365]	1368 [1357]	1368 [1360]	1368 [1360]	W (*W7″*), dA, CH b
1387 (1S) [1388]		[1376]			dG, dT
1426 (1) [1426]	1420 [1424]	1420 [1424]	1420 [1424]		dA, W (*W6*)
1449 (4) [1448]					CH_2 b
1459 (4) [1457]					CH_3 b, [amII′]
			1468	1460 [1457]	W (*W5*)
1486 (1)	1485 [1480]	1487 [1480]	1487 [1480]	[1484]	dG, dA, W (*W4*), F
1531 (0S)	1528	1533 [1531]			dC
1548 (2) [1547]		1546 [1551]	1546 [1546]	1546 [1546]	W (*W3*)
1578 (2) [1575]	1576 [1573]	1576 [1575]	1581 [1573]		dA, dG
1585 (2) [1585]					W (*W2*), F (*F8b*)
	1600				dG (ring + NH_2 b)
1606 (3) [1606]					F (*F8a*)
1621 (S) [1617]	1619 [1615]	1619 [1615]	1620 [1616]	1620 [1614]	W (*W1*)
1649 (10) [1648]					amI[I′]
	1650 [1656]	1649 [1657]	1647 [1649]		dT (C═O s)
1682 (S)		1682	1672 [1661]		Q, dG (C═O s)
				1772 [1769]	W(*W18* + *W16*)

[a] Raman band frequencies (in cm^{-1}) are for H_2O solutions of Pf3; corresponding Raman band frequencies for D_2O solutions of Pf3 are enclosed in square brackets ([ ]). Relative Raman band intensities (in parentheses) apply to the 514.5-nm excited spectrum of Pf3 in H_2O and are based upon a 0−10 scale, with 10 representing the intensity of the 1649 cm^{-1} band. Assignments are based upon detailed studies of unlabeled and isotopically labeled fd and Pf1 viruses and related model compounds (*10*−*17*, *19*−*24*). [b] Abbreviations: B, broad; S, shoulder; b, bend; s, stretch; bk, backbone; am, amide. Standard symbols are used for amino acids, deoxynucleosides, and chemical groups (PO_2^-, CC, CN, C═O, CH, CH_2, CH_3). Normal mode designations (in italics) are from refs *21* and *22*.

proteins, it would be helpful to identify distinct Raman markers for the arginyl guanido group [-N^{ϵ}H-C^{ζ}($N^{\eta 1}H_2$)-($N^{\eta 2}H_2$)$^+$]. Ongoing studies of guanido model compounds, including L-arginine and poly-L-arginine, indicate that a strong Raman marker can be expected near 1085 ± 10 cm^{-1} from the arginyl side chain (Tsuboi, M., Nakamura, K., and

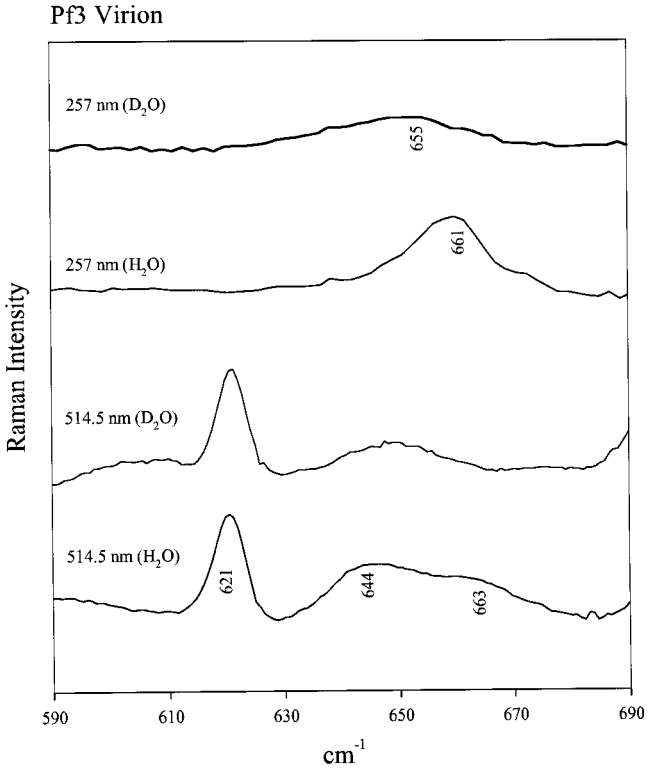

FIGURE 4: UVRR spectra (257 nm excitation, top two traces) and off-resonance Raman spectra (514.5 nm excitation, bottom two traces) in the interval 590−690 cm^{-1} of Pf3 virus (∼100 mg/mL) in H_2O and D_2O solutions. The 514.5-nm data demonstrate the well-characterized Raman marker of the C3′-*endo*/*anti* dG conformation, which is observed as a shoulder centered near ∼663 cm^{-1}. This dG marker undergoes a small deuteration shift to lower wavenumber (∼655 cm^{-1}), where it becomes overlapped by markers of the subunit methionine residue (Met 1) and C3′-*endo*/*anti* dT residues of packaged DNA to yield the resultant very broad band near ∼650 cm^{-1} (see text). The prominent Raman marker near 621 cm^{-1} is due to subunit phenylalanines (Phe-43, Phe-44) and serves as a convenient and accurate wavenumber and intensity standard (*19*). In the 257-nm excited UVRR spectrum, the corresponding marker of C3′-*endo*/*anti* dG is observed at ∼661 cm^{-1} for H_2O solution; the deuteration-shifted counterpart at ∼655 cm^{-1} is intrinsically very weak (*19*).

Thomas, G. J., Jr., manuscript in preparation). The 1085 cm^{-1} band is considered due to a normal mode of vibration associated primarily with stretching of guanido CN bonds. A modest deuteration shift (∼1085 → ∼910 cm^{-1}) is expected. As seen in Figure 2, Pf3 displays a candidate Raman marker near 1082 cm^{-1}, to which the guanido side chain of Arg-37 may contribute. However, the phosphates of packaged DNA (as well as other side chains of coat protein) are also expected to contribute Raman intensity in this interval; therefore, only a small intensity decrease with deuteration can be expected. The arginyl guanido assignment is further complicated by the fact that partial deuteration of the peptide main chain generates significant amide III′ intensity in the neighborhood of 946 cm^{-1}, which offsets the possible effect of guanido deuteration. Finally, it cannot be ruled out that the guanido moiety of Arg-37 could be protected from facile H → D exchange as a consequence of interaction with one or more neighboring side chains in the capsid assembly, including the putative cation−π interaction (*11*). Additional studies of model compounds will be required to assess whether arginyl guanido markers are sensitive (in wavenumber and/or intensity) to interaction with an indolyl π acceptor.

(*d*) *Other Raman Bands of the Capsid Subunit.* The phenylalanines of the Pf3 subunit (Phe-43 and Phe-44) contribute several prominent bands to the 514.5-nm Raman spectrum, as indicated in Table 2. The deuteration-insensitive band of low intensity at 827 cm^{-1} is of particular interest because of its potential for confusion with a tyrosine band of similar wavenumber and intensity in tyrosine-containing proteins (*28*). However, because the Pf3 subunit contains no tyrosine and because isotope labeling studies (*17*) clearly indicate a phenylalanine assignment, the 827 cm^{-1} band of Pf3 is attributed to residues Phe-43 and Phe-44. This revises an earlier proposal of assignment to packaged DNA (*16*).

The 905 cm^{-1} band of Pf3, like the corresponding band of Pf1 (904 cm^{-1}), is significantly weaker than that of fd (906 cm^{-1}), which can be explained by assignment to alanine side chains. The intensities correlate well with the alanine residue compositions of fd (20%), Pf1 (15%), and Pf3 (14%) coat proteins.

Structural Interpretation for Raman Markers of Packaged Pf3 DNA. (*a*) *Raman Markers of Deoxynucleoside Conformations*. Several Raman bands of the DNA bases have been established as indicators of deoxynucleoside conformation (*29*, *30*). Such conformational sensitivity arises typically from mechanical coupling (through the glycosyl bond) between vibrations of the purine or pyrimidine ring and the deoxyribose moiety (*31*). As an example we consider the spectral interval 590−690 cm^{-1}, which in principle contains Raman markers diagnostic of both dT and dG conformations (*29*). However, dG markers are intrinsically more intense than those of dT for both 514.5- (*29*) and 257-nm (*19*) excitations. Therefore, we focus initially on dG. The key dG conformational indicators are as follows: 682 ± 2 cm^{-1} (C2′-*endo*/*anti*), 671 ± 2 cm^{-1} (C2′-*endo*/*syn*), 664 ± 2 cm^{-1} (C3′-*endo*/*anti*), and 625 ± 3 cm^{-1} (C3′-*endo*/*syn*) (*29*). Figure 4 shows this region of the off-resonance Raman (514.5 nm excitation) and UVRR (257 nm excitation) spectra of Pf3 on a suitably expanded scale. It is clear that the only dG conformation marker consistent with both the 514.5- and 257-nm spectra of H_2O solutions of Pf3 is that for C3′-*endo*/*anti* dG, which accounts for most of the Raman and UVRR intensities located between 660 and 667 cm^{-1}. The accompanying band near 640−650 cm^{-1} can be attributed to the subunit methionine residue, Met 1. This is supported by 514.5-nm excited Raman spectra of H_2O and D_2O solutions of L-Met (data not shown) as well as by the deuteration effects shown in Figure 4. The latter can be understood as follows. The C3′-*endo*/*anti* dG marker (centered near ∼663 cm^{-1}) is slightly deuteration-shifted to lower wavenumber, as expected (*32*), resulting in increased overlap with the deuteration-insensitive methionine marker in the D_2O solution spectrum. A similar deuteration shift is anticipated for the dG marker in 257-nm excited UVRR spectra (*19*), which explains the observed data (Figure 4, top two traces).

We note that the data of Figures 2 and 4 are also consistent with dT residues of packaged Pf3 DNA adopting the C3′-*endo*/*anti* conformation, which should yield a strong marker at 777 cm^{-1} and a very weak couplet between 640 and 660 cm^{-1}; conversely, the data do not fit the band pattern expected for C2′-*endo*/*anti* dT (strong 668 ± 2 cm^{-1} marker) (*29*−*31*). Thus, C3′-*endo*/*anti* dT is presumed to contribute

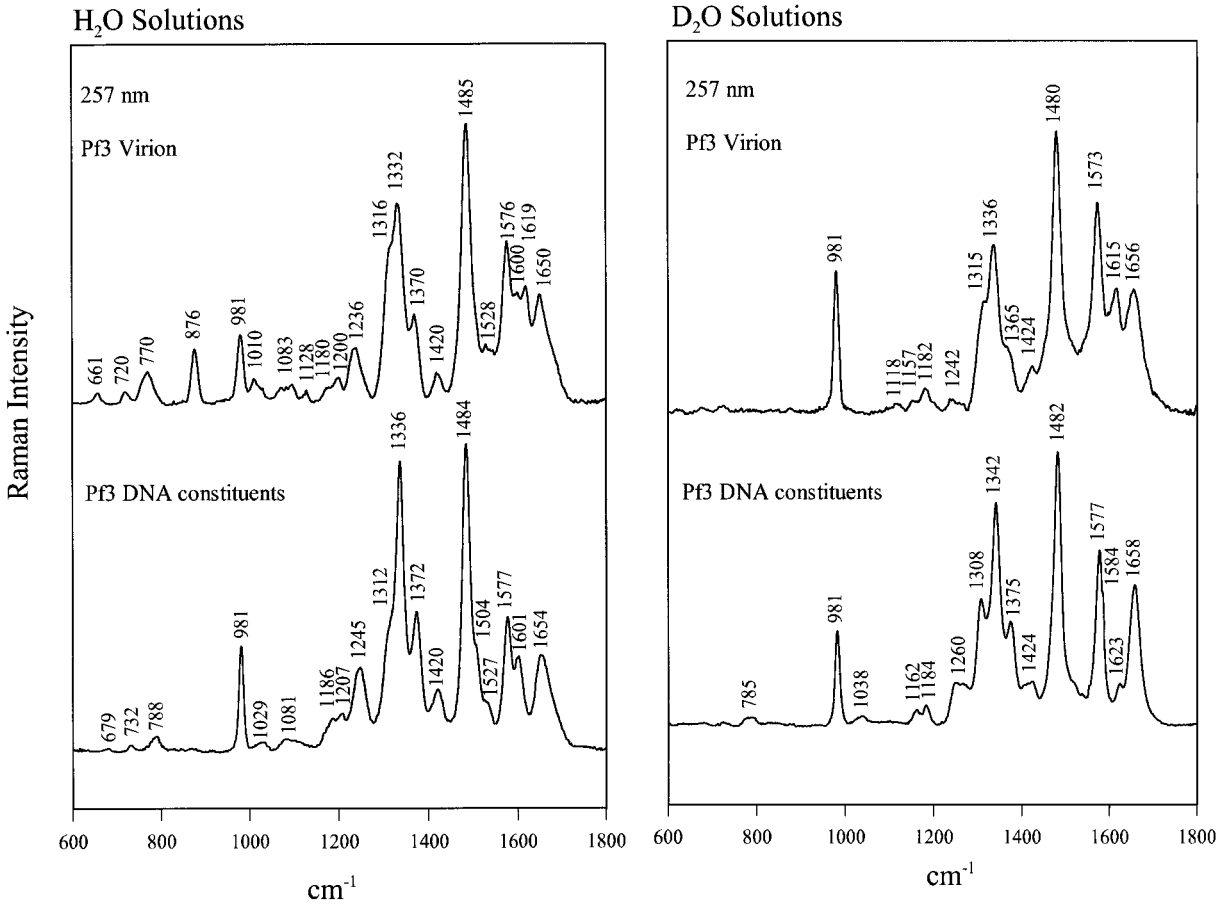

FIGURE 5: Left panel: UVRR spectra (257 nm excitation) of H_2O solutions of Pf3 (top) and a deoxynucleoside mixture having the same base composition (20% dA, 35% dT, 24% dG, 21% dC) as Pf3 DNA (bottom). Sample concentrations in terms of moles of DNA nucleotides are 1.04 and 0.80 mM, respectively; Na_2SO_4 concentrations are 91 and 200 mM, respectively. Right panel: UVRR spectra (257 nm excitation) of D_2O solutions of Pf3 (top) and a deoxynucleoside mixture having the same base composition as Pf3 DNA (bottom). Sample concentrations in terms of moles of DNA nucleotides are 0.56 and 0.80 mM, respectively; Na_2SO_4 concentrations are 80 and 200 mM, respectively.

Table 3: Raman Cross Sections and Hypochromic Ratios of Packaged Pf3 DNA[a]

Raman band (base)	$\sigma^{\text{Pf3 DNA}}$	$\sigma^{\text{Pf3 nucleotides}}$	γ
1332 (A)	47	75	0.63
1485 (A, G)	67	92	0.73
1576 (G, A)	31	42	0.75
1650 (T)	19	28	0.67

[a] Raman wavenumbers of packaged Pf3 DNA (column 1, cm^{-1}) and cross sections (columns 2 and 3, mb) are from the 257-nm excited UVRR spectra of Figure 5. Hypochromic ratios (column 4) were calculated using eq 3.

weak Raman intensity near ~650 cm^{-1}, which overlaps the methionine marker, and greater Raman intensity near 782 cm^{-1} (Figure 2). Moreover, the absence of appreciable Raman intensity near 668 cm^{-1} can be taken as evidence of the absence of C2′-*endo*/*anti* dT conformers in packaged Pf3 DNA. The prevalence of C3′-*endo*/*anti* dT is further supported by the distinctive deuteration-insensitive Raman (1244 cm^{-1}) and UVRR (1236 cm^{-1}) markers observed in Figures 2 and 3, respectively, which have been established as diagnostic of this dT conformation (*32*).

Deoxynucleoside conformations of the dA and dC residues of packaged Pf3 DNA cannot be inferred directly from the present Raman and UVRR data and the library of available marker bands (*29*). However, because dG and dT residues are distributed randomly and widely through the viral genome and because the genome is extended uniformly along the interior of the tubular capsid, all nucleotide residues are expected to encounter a similar protein interface and adopt similar conformations. It seems reasonable to conclude, therefore, that dA and dC residues such as dG and dT residues of encapsidated Pf3 DNA are in the C3′-*endo*/*anti* conformation.

(*b*) *UVRR Hypochromism and Base Stacking.* The most prominent bands in the 257-nm UVRR spectrum of Pf3 are due to ring vibrations of the packaged DNA bases (Table 2 and Figure 5). The intrinsic intensity, or Raman cross section, of a given band is subject to significant reduction (hypochromism) as a consequence of base stacking. This has been demonstrated previously for stacked base pairs of both protein-free ssDNA and dsDNA (*12*), for which the respective hypochromic ratios (γ, eq 3) are 0.45 ± 0.10 (intensity losses of 55 ± 10%) and 0.35 ± 0.10 (65 ± 10% intensity losses). Even more dramatic hypochromicity has been observed for the packaged ssDNA genome of fd, for which $\gamma = 0.25 \pm 0.04$ (75 ± 4% intensity loss). Conversely, relatively modest UVRR hypochromism ($\gamma \sim 0.85$, or ~15% intensity loss) is observed for the packaged ssDNA of Pf1 (*12*, *14*). These results can be explained in terms of the degree of base stacking that occurs in the respective DNA molecules. The relative magnitude of the UVRR hypochromic effect in a given filamentous virus thus provides a semiquantitative measure of the extent of "condensation" of the genome with encapsidation.

Figure 5 shows the data from which UVRR hypochromic effects can be calculated for the prominent bands of packaged Pf3 DNA. Table 3 lists these hypochromic effects for the strong bands near 1332, 1485, 1576, and 1650 cm^{-1}. Band assignments to ring vibrations of the indicated purines are well-established (*29*). The sensitivities of the corresponding Raman cross sections to base-stacking interactions are also well-documented (*12*). We find that for packaged Pf3 DNA, these bands suffer intensity losses of 31 ± 6% ($\gamma = 0.69 \pm 0.06$) in comparison to the "unperturbed" intensities ($\gamma = 1$) observed in the aqueous deoxynucleoside mixture of the same base composition. Thus, the hypochromic effects of packaged Pf3 DNA are relatively modest in comparison to those of packaged fd DNA ($\gamma = 0.25 \pm 0.04$) and double-stranded *B* DNA ($\gamma = 0.35 \pm 0.10$); yet, they are significantly more pronounced than those of packaged Pf1 DNA ($\gamma = 0.85$). In order of decreasing strength of base stacking (or decreasing degree of condensation), the available UVRR data suggest the following sequence:

fd DNA ($\gamma \sim 0.25$) > dsDNA > ssDNA > Pf3 DNA > Pf1 DNA > deoxynucleosides ($\gamma = 1$)

It is interesting to note that this scheme is generally consistent with earlier assessments of base stacking based upon UV absorption and CD spectra of filamentous viruses (*1*).

(*c*) *Thymine Carbonyl Hydrogen Bonding*. The prominent band centered at 1650 cm^{-1} in the 257-, 244-, and 238-nm excited UVRR spectra of Pf3 originates from a thymine ring vibration involving substantial C4═O and C5═C6 bond stretching and a lesser component of imino N3−H in-plane bending components (*31*). The shift to higher wavenumber (1650 → 1656 cm^{-1}) upon imino deuteration reflects uncoupling of the imino component. The 1650 cm^{-1} band is expected to be sensitive to the hydrogen bonding environment primarily of the C4═O acceptor group. Accordingly, the wavenumber value for the band center in packaged ssDNAs of fd, Pf1, and Pf3 virions provides a qualitative measure of the strength of hydrogen bonding of the thymine C4═O acceptor in these assemblies. The observed sequence, in order of decreasing strength of hydrogen bonding of the C4═O acceptor, is:

Pf1 (1640 cm^{-1}) > fd (1646 cm^{-1}) > Pf3 (1650 cm^{-1}) > thymidine (1652 cm^{-1})

We conclude that thymine C4═O groups in packaged Pf3 DNA form hydrogen bonds comparable in strength to those of the aqueous deoxynucleoside, but considerably weaker than those in packaged DNAs of Pf1 and fd virions.

(*d*) *Raman Indicators of Deuterium Exchange of Bases in Packaged Pf3 DNA.* Table 2 identifies a number of Raman and UVRR markers of packaged Pf3 DNA that are sensitive to the change of solvent from H_2O to D_2O. The observed deuteration shifts, e.g., 1332 → 1336, 1485 → 1480 and 1650 → 1656 cm^{-1}, reflect base amino and imino exchanges that are more rapid than the period of sample preparation and data collection protocols (~24 h). This contrasts with subunit peptide exchange, which is estimated to be no more than 50% complete in the same time interval and remains so up to the longest periods monitored (~100 h). Thus, at the experimental conditions employed (pH 7.8, 20 °C), the solvent readily penetrates the capsid to exchange DNA bases but does not catalyze exchange of the majority of α-helical peptide groups. Unprotected exchange of packaged DNA despite substantial exchange protection of the filament capsid is also observed in fd and Pf1 virions (*12*, *14*, *33*).

SUMMARY AND CONCLUSIONS

Class I (fd) and class II (Pf1, Pf3) filamentous viruses share certain morphological features: Several thousand copies of a small and hydrophobic α-helical subunit are assembled as a tubular capsid, the inner surface of which is lined with basic amino acid side chains. The capsid superhelix packages a covalently closed DNA single strand that is complemented electrostatically by the adjoining inner capsid surface. The key to virion assembly is presumably encoded in the sequence of the capsid subunit, which ensures the fidelity of subunit−subunit recognition and subunit−nucleotide interactions appropriate to the specific filament architecture. Nevertheless, different filamentous viruses exhibit fundamentally different spectroscopic properties, with respect to both the capsid subunit and packaged DNA. In previous Raman and UVRR studies (*12*, *14*, *16*, *34*, *35*), major differences in the organization of DNA in fd and Pf1 virions were reported. Here, we have demonstrated that Pf3 also differs from both Pf1 and fd in key spectroscopic features that relate to DNA structure and subunit environment. Although some of these characteristics were reported in earlier studies (*16*), the previous vibrational assignments were tentative and incomplete. The revised and more comprehensive assignments reported here reflect technical improvements in Raman instrumentation, including the combination of both off-resonance (514.5 nm) and ultraviolet resonance (257, 244, 238, and 229 nm) excitations. The comprehensive vibrational assignment scheme (Table 2) proposed for Pf3 has also been facilitated by the detailed isotopic labeling studies recently completed on the class I fd assembly by Overman and co-workers (*13*, *17*, *23*, *24*).

With respect to base stacking of packaged DNA, as monitored by UVRR hypochromism, Pf3 is intermediate between Pf1 and fd. Base stacking in encapsidated Pf3 DNA is also less extensive than occurs in either protein-free ssDNA or dsDNA. Surprisingly, however, the preferred deoxynucleoside conformation of packaged Pf3 DNA is C3′-*endo*/*anti*, i.e., the same as that of packaged fd DNA and distinct from the C2′-*endo*/*anti* conformation of packaged Pf1 DNA. Assuming that the deoxynucleoside conformation monitored by Raman (furanose pucker and glycosyl orientation) is related to intracapsid organization of DNA, the results provide evidence of different genome organizations in Pf1, Pf3, and fd. Apparently, the symmetry of the virion is not sufficient to determine DNA organization at the nucleotide level. Because C3′-*endo*/*anti* deoxynucleosides do not occur in the lowest energy state (*B* form) of protein-free DNA, we further conclude that this conformation is conferred through specific subunit−DNA interactions.

The anomalous Raman markers of Trp-38 in the Pf3 assembly, reported previously (*11*) and confirmed here, further define the distinctiveness of the Pf3 structure in relation to Pf1 and fd. These bands have been proposed as markers of indolyl interactions specific to the local environment of Trp-38 in native Pf3, possibly involving cation−π

interaction of the indolyl ring with the guanido group of Arg-37 (*11*). The feasibility of this interaction has been tested by polarized Raman spectroscopy of oriented Pf3 fibers and a structural model has been proposed (*15*).

ACKNOWLEDGMENT

We thank our colleagues Dr. Masamichi Tsuboi for sharing experimental results prior to publication and Dr. James M. Benevides for assistance in data collection and analysis. This is Paper LXIX in the series Structural Studies of Viruses by Raman Spectroscopy.

REFERENCES

1. Day, L. A., Marzec, C. J., Reisberg, S. A., and Casadevall, A. (1988) *Annu. Rev. Biophys. Biophys. Chem. 17*, 509−539.
2. Welsh, L. C., Symmons, M. F., Sturtevant, J. M., Marvin, D. A., and Perham, R. N. (1998) *J. Mol. Biol. 283*, 155−177.
3. Gonzalez, A., Nave, C., and Marvin, D. A. (1995) *Acta Crystallogr. 51D*, 792−804.
4. Makowski, L., and Russell, M. (1997) in *Structural Biology of Viruses* (Chiu, W., Burnett, R. M., and Garcea, R. L., Eds.) pp 352−380, Oxford University Press, New York.
5. Marvin, D. A., Hale, R. D., Nave, C., and Helmer Citterich, M. (1994) *J. Mol. Biol. 235*, 260−286.
6. Meijer, A. B., Spruijt, R. B., Wolfs, C. J. A. M., and Hemminga, M. A. (2000) *Biochemistry 39*, 6157−6163.
7. Kiefer, D., Hu, X., Dalbey, R., and Kuhn, A. (1997) *EMBO J. 16*, 2197−2204.
8. Thomas, G. J., Jr. (1999) *Annu. Rev. Biophys. Biomol. Struct. 28*, 1−27.
9. Matsuno, M., Takeuchi, H., Overman, S. A., and Thomas, G. J., Jr. (1997) *Biophys. J. 74*, 3217−3225.
10. Tsuboi, M., Suzuki, M., Overman, S. A., and Thomas, G. J., Jr. (2000) *Biochemistry 39*, 2677−2684.
11. Wen, Z. Q., and Thomas, G. J., Jr. (2000) *Biochemistry 39*, 146−152.
12. Wen, Z. Q., Overman, S. A., and Thomas, G. J., Jr. (1997) *Biochemistry 36*, 7810−7820.
13. Overman, S. A., and Thomas, G. J., Jr. (1999) *Biochemistry 38*, 4018−4027.
14. Wen, Z. Q., Armstrong, A., and Thomas, G. J., Jr. (1999) *Biochemistry 38*, 3148−3156.
15. Tsuboi, M., Overman, S. A., Nakamura, K., Rodriguez-Casado, A. R., and Thomas, G. J., Jr. (2001) *Biochemistry* (submitted for publication).
16. Thomas, G. J., Jr., Prescott, B., and Day, L. A. (1983) *J. Mol. Biol. 165*, 321−356.
17. Overman, S. A., and Thomas, G. J., Jr. (1995) *Biochemistry 34*, 5440−5451.
18. Russell, M. P., Vohník, S., and Thomas, G. J., Jr. (1995) *Biophys. J. 68*, 1607−1612.
19. Wen, Z. Q., and Thomas, G. J., Jr. (1998) *Biopolymers 45*, 247−256.
20. Fodor, S. P. A., Copeland, R. A., Grygon, C. A., and Spiro, T. G. (1989) *J. Am. Chem. Soc. 111*, 5509−5518.
21. Austin, J., Jordan, T., and Spiro, T. G. (1993) in *Advances in Spectroscopy* (Clark, R. J. H., and Hester, R. E., Eds.) Vol. 20A, pp 55−127, John Wiley and Sons, New York.
22. Takeuchi, H., and Harada, I. (1986) *Spectrochim. Acta 42A*, 1069−1078.
23. Overman, S. A., and Thomas, G. J., Jr. (1998) *J. Raman Spectrosc. 29*, 23−29.
24. Overman, S. A., and Thomas, G. J., Jr. (1998) *Biochemistry 37*, 5654−5665.
25. Thomas, G. J., Jr. (1985) *Spectrochim. Acta 41A*, 217−221.
26. Berjot, M., Marx, J., and Alix, A. J. P. (1987) *J. Raman Spectrosc. 18*, 289−300.
27. Gallivan, J. P., and Dougherty, D. A. (1999) *Proc. Natl. Acad. Sci. U.S.A. 96*, 9459−9464.
28. Siamwiza, M. N., Lord, R. C., Chen, M. C., Takamatsu, T., Harada, I., Matsuura, H., and Shimanouchi, T. (1975) *Biochemistry 14*, 4870−4876.
29. Thomas, G. J., Jr., and Tsuboi, M. (1993) *Adv. Biophys. Chem. 3*, 1−70.
30. Dijkstra, S., Benevides, J. M., and Thomas, G. J., Jr. (1991) *J. Mol. Struct. 242*, 283−301.
31. Tsuboi, M., Komatsu, K., Hoshi, J., Kawashima, E., Sekine, T., Ishido, Y., Russell, M. P., Benevides, J. M., and Thomas, G. J., Jr. (1997) *J. Am. Chem. Soc. 119*, 2025−2032.
32. Thomas, G. J., Jr., and Benevides, J. M. (1985) *Biopolymers 24*, 1101−1104.
33. Thomas, G. J., Jr., and Day, L. A. (1981) *Proc. Natl. Acad. Sci. U.S.A. 78*, 2962−2966.
34. Thomas, G. J., Jr., Prescott, B., Opella, S. J., and Day, L. A. (1988) *Biochemistry 27*, 4350−4357.
35. Day, L. A., Casadevall, A., Prescott, B., and Thomas, G. J., Jr. (1988) *Biochemistry 27*, 706−711.

BI0018887